Synthesis and structural characterization of nanocrystalline Fe-Ni-Zr-B alloy prepared by powder metallurgy

Abderrahmène SEKRI [a], Mohsen MHADHBI [a], Luiza ESCODA [b]
Juan Jose SUÑOL [b], Mohamed KHITOUNI [a *], Thabet MAKHLOUF [a]

[a] *Laboratoire de Chimie Inorganique (UR-11-ES-73), Faculté des Sciences de Sfax, Université de Sfax 1171, 3000-Sfax, Tunisia.*
[b] *Dep. de Fisica, Universitat de Girona, Campus Montilivi, Girona 17071, Spain.*

(Submitted: 28 February 2014, accepted: 12 August 2015)

Abstract: The present study reports on the formation of nanocrystalline Fe-Ni-Zr-B alloy using the mechanical alloying technique. Morphological, microstructural, structural and thermal characterizations of the powders milled several times were investigated by scanning electron microscopy, X-ray diffraction and differential scanning calorimetry. The patterns obtained were analyzed using the Rietveld refinement. The final products of the mechanically alloying process were a duplex nanostructure of Fe(Ni,Zr,B) and Fe_2B type boride nanocrystals. The increase of mechanical milling induced a continuous decrease in the crystallite sizes and an increase in the lattice strains. Recovery, recrystallization and ferro-paramagnetic transition at Curie temperature are revealed in the thermal analysis in the temperature range 35-700 °C.

Keywords: Fe-Ni-Zr-B alloy; X-ray methods; Nanostructures; High energy ball milling.

INTRODUCTION

Nanocrystalline (NC) materials have received increasing attention in recent research due to their attractive potential for application in a wide range of technological areas, including electronics, ceramics and industrial catalysts. These materials are characterized by a number of physical, mechanical, and magnetic properties that are superior to those of their conventional coarse-grained polycrystalline counterparts [1]. Various techniques have been developed over the past decades for the synthesis of NC materials, including mechanical alloying (MA). It is a solid-state powder processing technique that involves the mechanical milling or mixing of particles in ball milling equipments for the preparation of alloyed powders [1-3]. During ball milling, powders undergo a severe plastic deformation, which introduces a number of defects (dislocations, grain boundaries, vacancies, and interstitials) into the material. The constituents that favor the formation of a metastable structure can then "self assemble" into nanoscale grains. Additionally, since MA processing is carried out in the solid state, phase diagram restrictions do not seem to apply to the phases produced by the technique [1, 4, 5]. During the milling process, the repeated fracturing and cold welding of the powder particles lead to reactions between the solid components of the initial mixture. The mechanically stored enthalpy caused by internal strains due to the high density of dislocations and large fraction of grain boundaries can serve as a driving force for the formation of nanocrystalline and/or amorphous structures [1,6]. The interfacial components of the neighbouring atoms located at the grain boundaries can, therefore, contribute to improve the mechanical, physical, and magnetic properties of the milled material [7-9]. Knowledge of ternary additions to BCC alloy systems is one of the key points in

* Corresponding author: E-mail address: khitouni@yahoo.fr (M. Khitouni), Tel.: +216 98656430; Fax: +216 74276437.

understanding and controlling the mechanical properties of these materials and is critical to alloy design. Besides, the additions of transition metals (Ni, Zr, Cu, Ti, Cr, V, and Zr) have a significant influence on the final structure as well as on the crystallization of Fe -Al system [14-18]. Also, it has been reported that the addition of a small amount of B results in an improvement of soft magnetic properties [19]. In the present work, Fe, $Ni_{70}Zr_{30}$ and B powders were ball milled up to 42 hours. The structure evolution and thermal stability of the powders during ball milling were reported, aiming at clarifying the nanocrystallization process of the Fe-Ni-Zr-B alloy by MA method.

MATERIALS AND METHODS

The starting materials were pure Fe (purity of 99.7%, particle size of 20 µm), Ni_7Zr_3 (purity of 99.7%, particle size of 50 µm), and amorphous B (purity of 99.9%, particle size of 10 µm). These powders were mixed with the composition of $Fe_{80}(Ni_{70}Zr_{30})_{10}B_{10}$ (at.%). Mechanical alloying was carried out in a planetary ball mill (Fritsh P7) under an argon atmosphere. To prevent heating and sticking of the powder to container walls and the balls, and powder agglomeration during milling, the milling sequence was selected such as 10 min of milling followed by 5 min of idle period. Samples were collected from the vials after regular time intervals during milling for further investigations. The experiments were carried out in a hardened steel vial with five steel balls. The ball-to-powder ratio and the rotational speed were 5:1 and 700 rpm, respectively. A total of 10 g powder with process control agent was used in all MA runs. The morphological changes of the powder particles during the milling process were observed via scanning electron microscopy (SEM) using DSM960A Zeiss equipment. The mean powder particles size was estimated from SEM images of powder particles by image tool software. Phase identification, microstructural and structural evolutions were investigated by X-ray diffraction (XRD) with a Bruker D8 Advance diffractometer using (θ-2 θ) Bragg Brentano geometry and Cu-$K_{á}$ radiation (λ_{Cu} = 0.15406 nm). Structural parameters were determined through the Rietveld refinement of XRD patterns using the MAUD program [20]. Thermal analyses were performed by means of differential scanning calorimetry (DSC) instrument with a heating rate of 20 K/min up to 700 °C under constant Ar flow.

RESULTS AND DISCUSSIONS

1. Morphology and microstructure

Fig. 1 shows the morphology of milled samples obtained after different milling times. The particle morphology was characterized using a digital scanning electron microscope in the secondary electron image mode. After 2 h of milling the powder particles of mixed powders were noted to be almost equiaxed shape (Fig. 1a). After 12 h of milling, the average particle size decreased from 400 µm (at 2 h) to 320 µm (Fig. 1b). The milled powder particles became spherical shape because of the strong plastic deformation occurring at the very beginning of the milling process. Other particles were noted to undergo

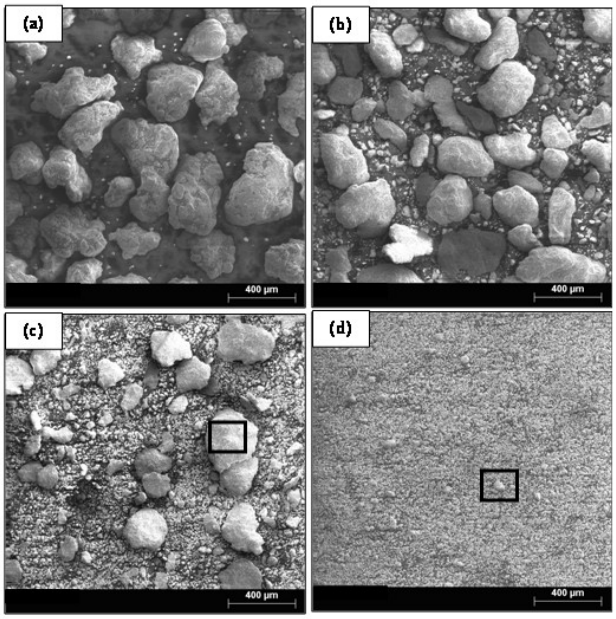

Fig. 1. Scanning electron micrographs (secondary electron image mode) corresponding to mechanically milled powders: (a) 2h, (b) 12h, (c) 18h and (d) 42h.

a fracture and a decrease in size of ~ 35 µm. After 18 h of milling, those particles were noted to undergo a fracture and a rapid decrease in size (Fig. 1c). After 42 h of milling, the particles were noted to exhibit a more regular, almost spherical, shape and to undergo a considerable increase in size reaching up to 20 µm (Fig. 1d). In addition, further milling led to a matrix of randomly welded thin layers of highly deformed particles. The typical EDX spectrums of the MA powders observed during 18 (Fig. 2c1) and 42 h (Fig. 2d1) show the characteristic peaks of powders milling (Fe, Ni and Zr). After milling of 42 h, one can see an oxygen peak, indicating the formation of metallic oxides in milled samples. The reason for the oxygen uptake can be related to oxygen introduced in the vessel after interruption and sampling. The non-apparent scaling of the amount of oxygen taken after 18 h of milling supports this explanation.

2. XRD analysis

Fig. 3 illustrates the XRD patterns of milled $Fe_{80}(Ni_{70}Zr_{30})_{10}B_{10}$ powder mixtures after different milling times. The multiple initial sharp peaks corresponded to the starting constituents. The X-ray pattern of the unmilled mixture powders is also presented for comparison. The powder samples were noted to undergo marked transformations during the milling process. Before milling, all XRD peaks related to Fe, Ni and Zr elements were observed. The diffraction peaks of B are not seen due its amorphous state. After 2 hours of milling, the peaks specific to α-Fe phase became less intense and their profiles became asymmetric and started to broaden. Rietveld refinement of the XRD patterns revealed BCC α-Fe (space group Im-3m; a=0.2865 (2) nm), cubic NiZr (space group Fm-3m; a=0.3529 (1) nm) and tetragonal Fe_2B (space group I4/mcm; a=0.5058 (1) nm and c=0.4203 (1) nm) and cubic $Fe_{23}B_6$ (space group Fm-3m; a=1.076 (2) nm) (Fig. 4a). According to the reduction of the NiZr peak intensities, it seems that there was only a crystallite size refinement. Thereby, one can suppose that only the reaction between Fe and B proceeds at this stage of milling because of the negative enthalpy of mixing (Δ H= -38 kJ/mol), their great affinity and similar diffusion coefficient. Different candidates are hold for this phase, as its indexation is quite difficult since the peaks are broad and have tiny intensities. A similar phase has been found from Mössbauer spectroscopy during the crystallization of FeZrB-based metallic glasses [21, 22]. The formation of the metastable Fe(B) phases, after 2 h of milling, might be related to the fact that

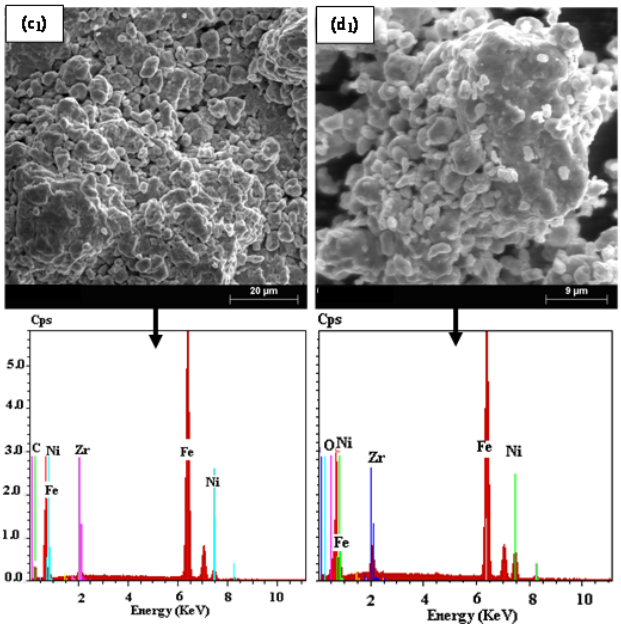

Fig. 2. Micrographs (c_1) and (d1) are the zoom regions of Fig.1c and 1d and the corresponding EDX spectrums.

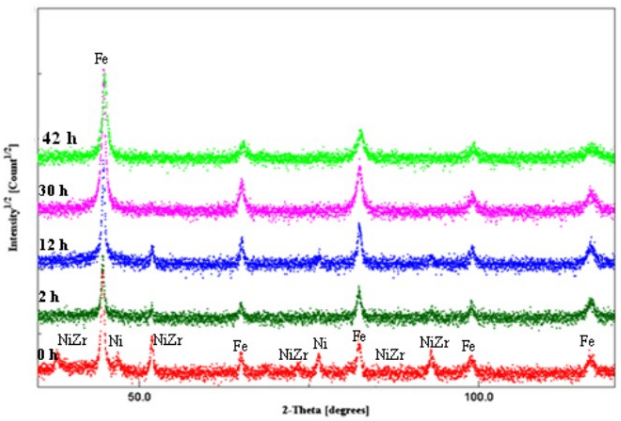

Fig. 3. X-ray diffraction patterns of mechanically alloyed Fe-Ni-Zr-B powders as a function of the milling time.

during MA the atomic diffusivity is enhanced through the creation of a large amount of structural defects. Consequently, metastable phases may well be the first product of the solid state reactions. The XRD patterns of the powders milled for 12 h demonstrate the same peaks. Accordingly, the Rietveld refinement has been performed by the introduction of four phases: bcc Fe rich phase with lattice parameter a=0.2845 (2) nm and space group Im-3m, cubic NiZr with unit cell a=0.3527 (1) nm and space group Fm-3m, tetragonal Fe_2B a=0.5152(1) nm and c=0.4183 (2) nm and space group I4/mcm and orthorhombic Fe_3B with space group Pbnm and unit cells a=0.5372 (1) nm, b=0.6534 (1) nm and c=0.4307 (1) nm (Fig. 4b). The increase of the main α-Fe diffraction peak intensity after 12 h of milling (see the Fig. 3) as well as the formation of the Fe_3B type boride can be correlated to the decomposition of the $Fe_{23}B_6$ type boride through the following reaction: $Fe_{23}B_6 \rightarrow 5Fe + 6Fe_3B$ [23]. As the milling process progresses up to 30 h, the diffraction peaks of NiZr disappear completely while those of the other phases show considerable broadening indicating the complete dissolution of NiZr in the Fe matrix and the intense refinement of the microstructure.

The best Rietveld refinement of the powders milled for 30 h was obtained with three phases: bcc-Fe(Ni,Zr,B) phase, Fe_2B and Fe_3B type borides (Fig. 4c). Finally, after milling for 42 h, the Rietveld refinement of the XRD patterns demonstrates that the powder consisted of bcc-Fe(Ni,Zr,B) phase and Fe_2B type boride (Fig. 4c). The favourite formation of the Fe_2B type boride can be related to the crystallite size refinement and the structural defects. Indeed, since nanocrystalline materials contain a very large fraction of atoms at the grain boundaries, the numerous interfaces provide a high density of short-circuit diffusion paths and thus, they are expected to exhibit an enhanced diffusivity. Consequently, the diffusion through the grain boundaries controls the rate of some precipitation reactions in the solids [24, 25]. On the other hand, the solid state disordering requires the existence of a high level of defects (vacancies,

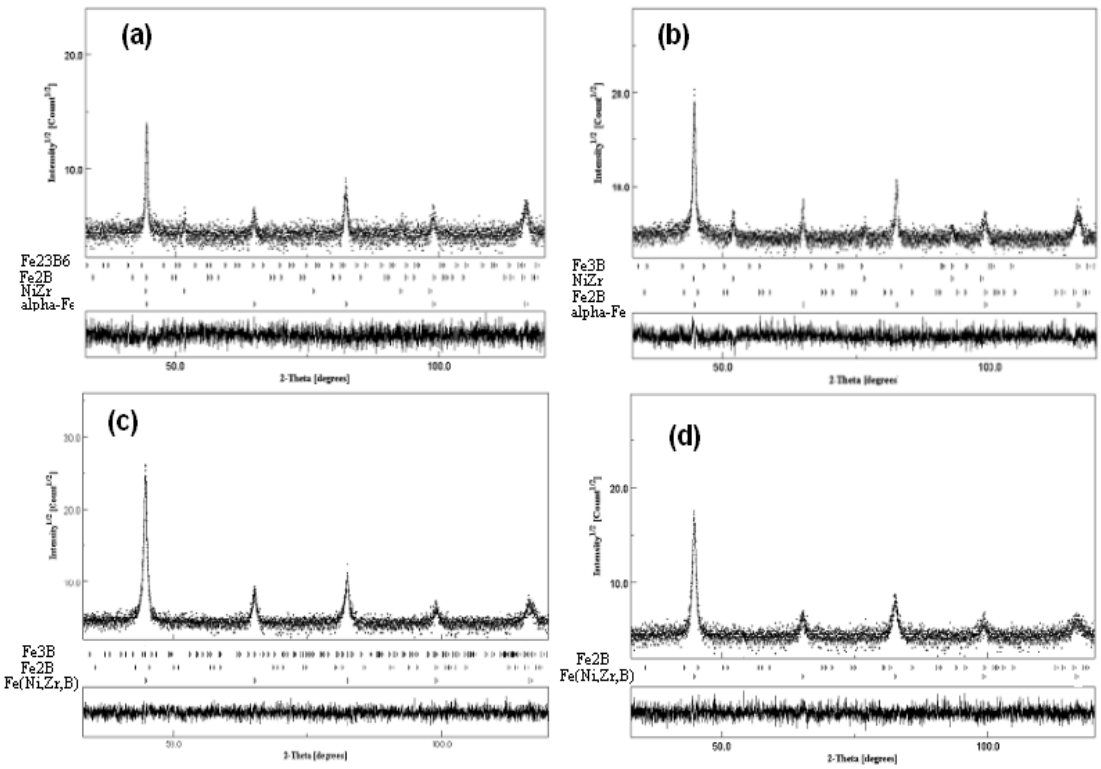

Fig. 4. Rietveld refinement of the XRD patterns of the powders milled for (a) 2 h, (b) 12 h, (c) 30 h and (d) 42 h.

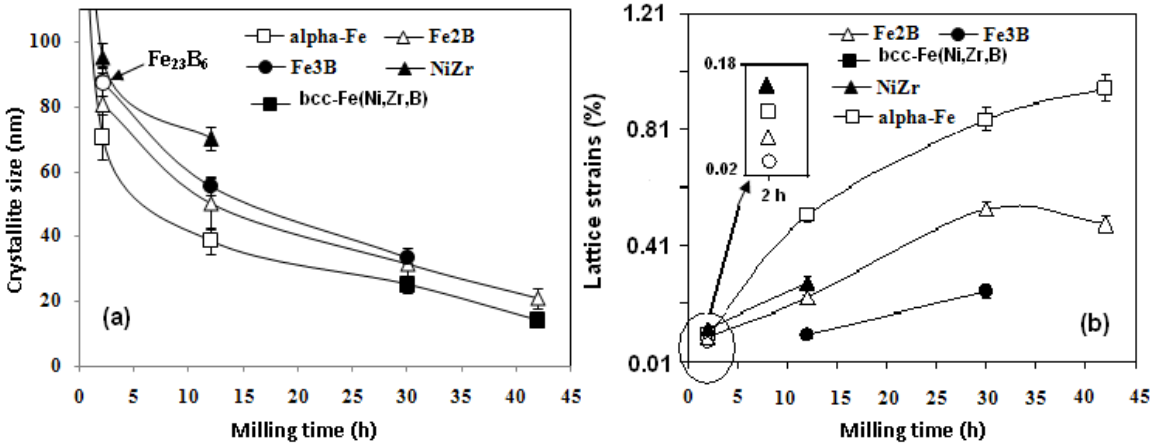

Fig. 5. Dependence of the calculated (a) crystallite sizes and (b) lattice strains of the identified phases on the milling time.

interstitials, dislocations…). Accordingly, the severe plastic deformation strongly distorts the unit cell structures making them less crystalline. The powder particles are subjected to continuous defects that lead to a gradual change in the free energy of the crystalline phases above those of amorphous ones and hence, to a disorder in atomic arrangement. The decrease of the amplitude and the increase of the broadening of the Bragg peaks with milling time can be explained by the contribution of the effective crystallite size and an increase of the atomic level strain because of heavy plastic deformation. Fig.5a shows the dependence of the calculated crystallite sizes and lattice strains on the milling time. One can observe the sharp decrease of the crystallite sizes of α-Fe and NiZr phases smaller than 100 nm after 2 h of milling. It is worth noting that the character of nanocrystalline structure under certain conditions of deformation is dependent on the crystalline structure. For nanocrystalline structures observed in BCC metals, the final crystallite size is determined by the evolution from dislocation cell structure containing dislocation cells/low-angle boundaries to a nearly uniform random structure consisting of nanocrystals with high-angle boundaries [26-28]. While, in the case of FCC metals, the low crystallite size is explained by the competition between the levels of stress produced by a milling device, and the large degree of dynamic recovery in the milled material [26-29]. After 2 h of milling, the measured crystallite size is 80.5 and 87.5 nm for Fe_2B and $Fe_{23}B_6$, respectively. After 30 h of milling, the crystallite size of α-Fe, Fe_2B and Fe_3B (crystallized after 12 h with a size of 55.5 nm) diminishes to about 25, 31.5 and 33.5, respectively. Then, after 42 h of milling, the crystallite size of the bcc-Fe solid solution and Fe_2B phases decreases with increasing milling time to about 14 and 21 nm, respectively. In the same time, the lattice strains of the bcc-Fe solid solution indicate a gradual increase from about 0.02% (after 2 h milling) to 0.95 % (after 42 milling) as increasing milling time (Fig. 5b). In general, lattice strains caused by MA are commonly attributed to the generation and movement of dislocations [30]. Fecht [31] claimed that the generation and the movement of dislocations could decrease grain size. Rawers and Cook [32] showed that the strain on the nanograin boundary could extend into nanograin, expanding the lattice. In the case of the Fe_2B type boride the lattice strains values increases up to 0.48 % for 42 h milling.

3. Thermal stability

In order to study the thermal stabilities of the nanostructured milled powders, isothermal heating was carried out. Fig. 6 shows typical isothermal heating DSC traces

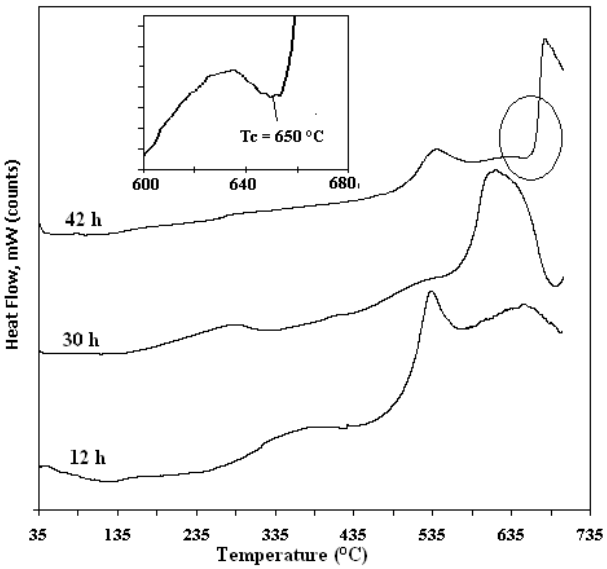

Fig. 6. DSC scans of the MA Fe-Ni-Zr-B powders at selected (at heating rate of 20 K/min).

for $Fe_{80}(Ni_{70}Zr_{30})_{10}B_{10}$ alloy powders milled for 12, 30 and 42 h. All DSC scans show several reactions on heating. After 12 h of milling, the low temperature exothermal process (below 400° C) can be a signature of recovery of stress, that is, mainly deformation energy stored during the milling process. At high temperature, two overlapped exothermal reactions occur in a wide range and characteristic of structural transformations, such as reordering or crystallization/ recrystallization. The same observations were shown by Pilar et al. [33] and Sunol et al [34] in the case of $Fe_{60}Co_{10}(Ni_{70}Zr_{30})_{15}B_{15}$ and $Fe_{60}Ni_{14}Zr_6B_{20}$, respectively. The late processes have generally well defined activation energy. On the contrary, recovery may be modeled by use of a wide spectrum of activation energies of the relaxation time [35]. As increasing the temperature, two or three crystallization processes appear related with the crystal growth and reordering of the crystalline phases. Moreover, one can see a slight change in temperature associated to the decrease of the crystallite size with increasing milling time. Furthermore, the DSC scan of the powder milled for 42 h exhibits an endothermic peak at T = 650 °C. This can be related to the Curie temperature (Tc= 650 °C) temperature of the identified disordered bcc-Fe (Ni,Zr,B) phase. DSC detects the Curie

Table I. Identified phases and the structural characteristics in the investigated FeNiZrB alloy as a function of milling time.

Milling time (h)	**phases**	**Space Groupe**	**Lattice parametter (nm)**		
	a	**b**	**c**		
2	α-Fe	Im-3m	0.2865		
	NiZr	Fm-3m	0.3529		
	Fe23B6	Fm-3m	1.076		
	Fe2B	I4/mcm	0.5058	0.5058	0.4203
12	á-Fe	Im-3m	0.28645		
	NiZr	Fm-3m	0.3527		
	Fe2B	I4/mcm	0.5152		0.4183
	Fe3B	Pnma	0.53729	0.65341	0.43708
30	Fe- (Ni,Zr,B)	Im-3m	0.28772	-	-
	Fe2B	I4/mcm	0.5267		0.4141
	Fe3B	Pnma	0.53510	0. 65031	0. 4205
42	Fe-(Ni,Zr,B)	Im-3m	0.2874	-	-
	Fe2B	I4/mcm	0.5311	0.5311	0.4001

temperature as a change in heat flow and due to the small amount of energy associated with this transition. An endothermic reaction occurs just below the Curie temperature as energy absorbed by the sample to induce randomization of the magnetic dipoles. An exothermic reaction occurs directly after the Curie temperature since no further energy is needed for randomization. This exothermic event can be related to the crystallization processes of the α-Fe(Ni,Zr,B) and Fe_2B highly disordered phases as detected by X-ray diffraction. Moreover, new mechanically alloyed compositions are under study to analyze precursor influence in the MA process and in the thermal stability of the alloys.

CONCLUSION

A nancrystalline Fe(Ni,Zr,B) alloy and Fe-boride were revealed after milling of a mixture of crystalline á-Fe, Ni_7Zr_3 and amorphous B powders up to 42 hours. Structural evolution was followed by XRD using Rietveld refinement. The increase of the milling time favours the reduction of the nanocrystalline size (about 18 nm) and an increase of the lattice strains (0.48-0.95 %). Several exothermic effects are associated with the structural relaxation, grain growth and recrystallization phenomena induced by heating in the calorimeter.

Acknowledgements: Financial support from ACID project is acknowledged. Authors would like to thank Xavier Fontrodona Gubau for her XRD support.

REFERENCES

[1] Suryanarayana C, Mechanical alloying and milling, *Prog. Mater Sci*. 46 (**2001**) 1.
[2] Koch CC, Cavin OB, McKamey CG, Scarborough JO, Preparation of ‘‘amorphous’’ $Ni_{60}Nb_{40}$ by mechanical alloying Appl. *Phys. Lett*. 43 (**1983**) 1017.
[3] Schlorke N, Eckert J, Schultz L, Synthesis of Multicomponent Fe-Based Amorphous Alloys with Significant Supercooled Liquid Region by Mechanical Alloying, *Mater. Sci. and Eng*. A226-228 (**1997**) 425.
[4] C. Suryanarayana, Mechanical Alloying and Milling, *Marcel Dekker*, New York, **2004**.
[5] M. Mhadhbi, M. Khitouni, L. Escoda, J.J. Sunol, M. Dammak, Microstructure evolution and mechanical properties of nanocrystalline FeAl obtained by mechanical alloying and cold consolidation, *J. of Alloys and Comp*. 509 (**2011**) 3293-3298.
[6] M. Sherif El-Eskandarany, “Mechanical Alloying for Fabrication of Advanced Engineering Materials”, *Noyes Publications*/William Andrew Publishing, Norwich, NY, **2001**.
[7] C. Suryanarayana, C.C. Koch, in: C. Suryanarayana (Ed.), *Non-equilibrium Processing of Materials*, Pergamon, New York (**1999**) 313-344.
[8] E.S. Park, D.H. Kim, Phase separation and enhancement of plasticity in Cu-Zr-Al-Y bulk metallic glasses, *Acta Mater*. 54 (**2006**) 2597.
[9] A.I. Salimon, A.M. Korsunsky, E.V. Shelekhov, T.A. Sviridova, S.D. Kaloshkin, V.V. Tcherdynsev, et al., Crystallochemical aspects of solid state reactions in mechanically alloyed Al-Cu -Fe quasicrystalline powders, *Acta Mater*. 49 (**2001**) 1821.
[10] M. Krifa, M. Mhadhbi, L. Escoda, J.M. Güell, J.J. Sunol, N. Llorca-Isern, C. Artieda-Guzman, M. Khitouni, Nanocrystalline $(Fe_{60}A_{l40})_{80}Cu_{20}$ alloy prepared by mechanical alloying, *J. of Alloys and Comp*. 554 (**2013**) 51-58.
[11] I. Baker, E.P. George, in: S.C. Deevi, V. Sikka (Eds.), Proceedings of the International Symposium on Nickel and Iron Aluminides, *The Minerals, Metals and Materials Society*, Warrendale, (**1997**) 145-156.
[12] P.F. Tortorelli, J.H. DeVan, Behavior of iron aluminides in oxidizing and oxidizing/sulfidizing environments, *Mater. Sci. Eng*. A 153 (**1992**) 573-577.
[14] Z. Shuzhu, W. Wenwu, Mechanical alloying characteristic and thermal stability of Al78Fe20Zr2 amorphous powders, *Rare Metals* 29 (**2010**) 226.
[15] V.I. Fadeeva, V.K. Portnoy, Y.V. Baldokhin, G.A. Kotchetov, H. Matyja, Nanocrystalline bcc solid solutions of Al-Fe-V system prepared by mechanical alloying, *Mater*. 12(5) (**1999**) 625.
[16] S. Sharma, R. Vaidyanathan, C. Suryanarayana, Criterion for Predicting the Glass-Forming Ability of Alloys, *Appl Phys Lett*., 90 (**2007**) 111915-1 to 111915-3.
[17] C. Stiller, J. Eckert, S. Roth, R. Schafer, U. Klement, L. Schulz, Mechanically alloyed Fe-Zr-(B,Cu) alloys: effect of composition and heat treatment on the microstructure and the magnetic properties, *J. Non-Cryst Solids* 205-207 (**1996**) 620.
[18] J.S. Garitaonandia, P. Gorria, L. Fernandez-Barquin, J.M. Barandiarán, Low temperature magnetic properties of Fe nanograins in an amorphous Fe-Zr-B matrix, *Phys Rev* B 61 (9) (**2000**) 6150-6155.
[19] A. Inoue, K. Kobayashi, J. Kanehira, Masumoto, Mechanical properties and thermal stability of (Fe, Co, Ni)-M-B (M=IV, V, VI group transition

metals) amorphous alloys with low boron concentration Sci. Rep. Res Inst. Tohoku University, Series A (*Physics, Chemistry, and Metallurgy*), June 29 (2) (**1981**) 331-342.
[20] L. Lutterotti, *MAUD CPD Newsletter*, IUCr, (**2000**) 24.
[21] A. Grabias, M. Kopcewicz and D. Oleszak, Phase transformations in the Fe(Co,Ni)ZrB alloys induced by ball milling, *J. of Alloys and Comp*. 339 (**2002**) 221-229.
[22] T. Shinjo, F. Itoh, H. Takaki, et al., Fe57 Mossbauer Effect in Fe2B, FeB and Fe3C, *J. Phys. Soc. Jpn*. 19 (**1964**) 1252.
[23] C. Gomez-Polo, Magnetic properties of Fe-based soft magnetic nanocrystalline alloys, *J. Magn. Magn. Mater*. 320 (**2008**) 1984.
[24] A.R. Yavari, O. Drbohlav, Ferromagnetic Nanocrystalline Materials from Amorphous Precursors, *Mater. Trans. JIM 36* (7) (**1995**) 896.
[25] S. Souilah, S. Alleg, C. Djebbari, R. Bensalem, J.J. Sunol, Magnetic and microstructural properties of the mechanically alloyed $Fe_{57}Co_{21}Nb_7B_{15}$ powder mixture *Materials Chemistry and Physics* 132 (**2012**) 766- 772
[26] M. Mhadhbi, M. Khitouni, M. Azabou, A. Kolsi, Characterization of Al and Fe nanosized powders synthesized by high energy mechanical milling, *J. of Mater. Charact*. 59 (**2008**) 944-950.
[27] D.L. Zhang, Processing of advanced materials using high-energy mechanical milling , *Progress in Materials Science* 49 (**2004**) 537-560.
[28] E. Gaffet, G. Le Caër, in: H.S. Nalwa (Ed.), Mechanical Processing for Nanomaterials, *Encyclopedia of Nanoscience and Nanotechnology*, 5, American Scientific Publishers (**2004**) 91-129.
[29] A.I. Salimon, A.M. Korsunsky, A.N. Ivanov, The character of dislocation structure evolution in nanocrystalline FCCNi-Co alloys prepared by high -energy mechanical milling, *J. of Mater. Sci. and Eng*. A 271 (**1999**) 196-205.
[30] F.A. Mohamed A dislocation model for the minimum grain size obtainable by milling. *Acta Mater* 51 (**2003**) 4107-19.
[31] Fecht HJ. Nanostructure formation by mechanical attrition. Nanostruct Mater 6 (1-4) (1995) 33-42.
[32] Rawers J, Cook D. Influence of attrition milling on nano-grain boundaries. *Nanostruct. Mater* 11 (**1999**) 331-342.
[33] M. Pilar, L. Escoda, J. J. Sunol, J. M. Grenech, Magnetic study and thermal analysis of a metastable Fe-Zr-based alloy: Influence of process control agents, *J of magnetism and magnetic mater*. 320 (**2008**) e823-e827.
[34] J. J. sunol, T. Pradell, N. Clavaguera, M. T. Claveguera-Mora, Mössbauer spectroscopy study of the crystallization behavior of Fe-Ni-P-Si amorphous powders prepared by ball milling, *Mater Sci*. From 360 (3) (**2001**) 525.
[35] M.T. Clavaguera-Mora, J.J. Suñol and N. Clavaguera, Relaxation kinetics of mechanically alloyed powders. Fe-Ni-Si-P: A case study, *J. Metast. Nanocryst. Mater*., 10 (**2001**) 459.